

The  $I(V)$  data became more asymmetric as the tip-cluster separation increased. We cannot at present determine whether the nonzero value of  $Q_0$  is related to work-function differences between tip and cluster or to the local chemical environment of the XYL-Au cluster nanostructure.

Gold clusters prepared by the MECS are crystalline and have been shown to orient with their (111) facets parallel to atomically flat substrates (13). If we assume that these clusters are truncated octahedrons, we can estimate the resistance of a single XYL molecule from measurements of  $R_1$  for an Au cluster-XYL SAM-Au substrate nanostructure (16). From the Coulomb staircase data, the resistance of a single XYL molecule is estimated to be  $18 \pm 12$  megohms. This result can be compared with a theoretical calculation of the resistance of an XYL molecule bonded between two Au surfaces, in which  $R_{XYL}$  was found to be  $4.5 \pm 0.50$  megohms. This resistance was calculated from the Landauer formula  $R = (h/2e^2)T_T$ . Here,  $h$  is Planck's constant and  $T_T$  is the transmission coefficient through an XYL molecule sandwiched between two Au surfaces; we calculated it using an extended Hückel molecular orbital description of the molecule (18).

## REFERENCES AND NOTES

- H. Grabert and M. H. Devoret, Eds., *Single-Charge Tunneling* (Plenum, New York, 1992).
- I. O. Kulik and R. I. Shekhter, *Sov. Phys. JETP* **41**, 308 (1975).
- A. E. Hanna and M. Tinkham, *Phys. Rev. B* **44**, 5919 (1991).
- M. Amman, R. Wilkins, E. Ben-Jacob, P. D. Maker, R. C. Jaklevic, *ibid.* **43**, 1146 (1991).
- J. F. Rabolt, F. C. Burns, N. L. Schlötter, J. D. Swalen, *J. Chem. Phys.* **78**, 946 (1983); R. G. Snyder, H. L. Strauss, C. A. Elliger, *J. Phys. Chem.* **86**, 5145 (1982); R. G. Nuzzo and D. L. Allara, *J. Am. Chem. Soc.* **105**, 4481 (1983); J. A. Chapman and D. Tabor, *Proc. R. Soc. London Ser. A* **242**, 96 (1957); H. A. Biebuyck and G. M. Whitesides, *Langmuir* **9**, 1766 (1993); Y.-T. Kim, R. L. McCarley, A. J. Bard, *ibid.* **8**, 1941 (1993).
- J. M. Tour et al., *J. Am. Chem. Soc.* **117**, 9529 (1995).
- We assigned the observed RAIR bands for XYL-Au using the system of substituted benzene normal modes, **1** through **20a,b**, with symmetry labels appropriate for the local symmetry ( $D_{2h}$ ) of the XYL ring system (8):  $3022\text{ cm}^{-1}$  (**20b**  $b_{2g}$ ),  $2921\text{ cm}^{-1}$  ( $\nu_{as}$   $\text{CH}_2$ ),  $1511\text{ cm}^{-1}$  (**19a**  $b_{1u}$ ),  $1423\text{ cm}^{-1}$  (**19b**  $b_{2u}$ ), and  $1263\text{ cm}^{-1}$  (**13**  $b_{1u}$ ). For BPD-Au, assignments again follow the system of substituted benzene normal modes, **1** through **20a,b**, with symmetry labels appropriate for the local symmetry ( $C_{2v}$ ) of the BPD ring system (8):  $3045\text{ cm}^{-1}$  (**2 a**),  $3021\text{ cm}^{-1}$  (**7b**  $b_2$ ),  $1592\text{ cm}^{-1}$  (**8a**  $a_1$ ),  $1474\text{ cm}^{-1}$  (**19a**  $a_1$ ),  $1406\text{ cm}^{-1}$  (**19b**  $b_2$ ),  $1387\text{ cm}^{-1}$  (**19b**  $b_2$ ),  $1106\text{ cm}^{-1}$  (**18b**  $b_2$ ), and  $1000\text{ cm}^{-1}$  (**18a**  $a_1$ ). The RAIR spectra did not display the expected  $\nu(\text{S-H})$  mode, observed at  $2555\text{ cm}^{-1}$  in a bulk solid spectrum in KBr. Possible explanations are that this mode would be nearly parallel to the surface and hence forbidden by surface selection rules or that the thiols oxidized to disulfides when the sample was transferred from the inert atmosphere where the SAMs were prepared to the RAIR chamber.
- G. Varsanyi, *Assignments for Vibrational Spectra of Seven Hundred Benzene Derivatives* (Wiley, New York, 1974), vol. 1.

- S.-C. Chang, I. Chao, Y.-T. Tao, *J. Am. Chem. Soc.* **116**, 6792 (1994).
- S. R. Wasserman, H. Biebuyck, G. M. Whitesides, *J. Mater. Res.* **4**, 886 (1989).
- R. S. Bowles, J. J. Kolstad, J. M. Calo, R. P. Andres, *Surf Sci.* **106**, 117 (1981); S. B. Park, thesis, Purdue University (1988).
- A. N. Patil, D. Y. Paithankar, N. Otsuka, R. P. Andres, *Z. Phys. D* **26**, 135 (1993).
- W. Mahoney, S. T. Lin, R. P. Andres, *Mater. Res. Soc. Symp. Proc.* **355**, 83 (1995); T. Castro et al., *J. Vac. Sci. Technol. A* **7**, 2845 (1989).
- R. Piner and R. Reifenger, *Rev. Sci. Instrum.* **60**, 3123 (1989).
- T. G. Miller, M. W. McElfresh, R. Reifenger, *Phys. Rev. B* **48**, 7499 (1993).
- M. Dorigi, J. Gomez, R. Osifchin, R. P. Andres, R. Reifenger, *ibid.* **52**, 9071 (1995).

- In making this estimate, we assumed a dielectric constant for the XYL dithiol of 1.5.
- M. P. Samanta, W. Tian, S. Datta, J. I. Henderson, C. P. Kubiak, *Phys. Rev. B* **53**, 7626 (1996).
- D. W. Pashley, M. J. Stonewell, M. H. Jacobs, T. J. Law, *Philos. Mag.* **10**, 127 (1964).
- This research was funded in part by the Army Research Office under grant DAAL03-G-0144. S.F. and J.I.H. acknowledge Purdue Research Foundation graduate fellowships. T.B., R.P.A., and R.R. received funding from the National Science Foundation. The visit of J. Gomez from Universidad Autonoma de Madrid proved pivotal in acquiring reliable  $I(V,z)$  data. We also thank S. Datta and D. Janes for many useful discussions and T. Henderson for preparing figures.

21 November 1995; accepted 1 April 1996

## Filled Skutterudite Antimonides: A New Class of Thermoelectric Materials

B. C. Sales,\* D. Mandrus, R. K. Williams

A class of thermoelectric materials has been synthesized with a thermoelectric figure of merit  $ZT$  (where  $T$  is temperature and  $Z$  is a function of thermopower, electrical resistivity, and thermal conductivity) near 1 at 800 kelvin. Although these materials have not been optimized, this value is comparable to the best  $ZT$  values obtained for any previously studied thermoelectric material. Calculations indicate that the optimized material should have  $ZT$  values of 1.4. These ternary semiconductors have the general formula  $\text{RM}_4\text{X}_{12}$  (where R is lanthanum, cerium, praseodymium, neodymium, or europium; M is iron, ruthenium, or osmium; and X is phosphorus, arsenic, or antimony) and represent a new approach to creating improved thermoelectric materials. Several alloys in the composition range  $\text{CeFe}_{4-x}\text{Co}_x\text{Sb}_{12}$  or  $\text{LaFe}_{4-x}\text{Co}_x\text{Sb}_{12}$  ( $0 < x < 4$ ) have large values of  $ZT$ .

The coupling between heat and electrical currents in a solid has fascinated scientists since the early experiments of Lenz in 1838. He placed a drop of water on the junction of Bi and Sb metal wires. Passing an electric current through the junction in one direction caused the water to freeze, and reversing the current caused the ice to melt rapidly; a thermoelectric refrigerator was thus created. This phenomenon remained little more than a curiosity until the early 1950s, when it was found that doped semiconductors could increase the efficiency of thermoelectric devices to values that allowed their practical use in specialized applications in which reliability was more important than economy (1). Today, portable thermoelectric coolers can be powered from a car battery for food storage or can be energized from a computer power supply to provide active cooling for high-density integrated electronic chips. A closely related thermoelectric effect produces electricity if a temperature gradient is established across the device. These thermoelectric generators are used as power sources for many of NASA's

deep space probes (2) and are currently of interest in the automobile industry for power generation from exhaust and engine heat.

Materials used today in thermoelectric devices— $\text{Bi}_2\text{Te}_3$ - $\text{Sb}_2\text{Te}_3$  alloys for refrigeration and Si-Ge alloys for power generation at elevated temperatures—were developed in the early 1960s. The main drawback of thermoelectric devices is their efficiency, which depends on materials properties through the dimensionless parameter  $ZT$ , where  $T$  is the temperature and  $Z = S^2/\kappa\rho$  (where  $S$  is the thermopower or Seebeck coefficient,  $\rho$  is the electrical resistivity, and  $\kappa$  is the thermal conductivity). Although many materials have been investigated in the intervening 35 years, the efficiency of thermoelectric devices has not improved significantly. However, theory shows that there is no fundamental maximum limit to  $ZT$  (1, 2). Moreover, several plausible extrapolations, based on the use of optimum values for known materials, indicate that  $ZT$  values of 2 to 4 are possible (1, 3). A value of  $ZT = 3$  would make thermoelectric home refrigerators economically competitive with traditional compressor-based refrigerators. We present initial experimental data on a new class of thermoelectric materials, filled skutterudites. Although these materials are clearly unoptimized, they ex-

B. C. Sales and D. Mandrus, Solid State Division, Oak Ridge National Laboratory, Oak Ridge, TN 37831, USA. R. K. Williams, Metals and Ceramics Division, Oak Ridge National Laboratory, Oak Ridge, TN 37831, USA.

\*To whom correspondence should be addressed.

hibit values of  $ZT$  comparable to the best values previously attained.

The word "skutterudite" is derived from a town in Norway where minerals with this structure, such as  $\text{CoAs}_3$ , were first discovered. Compounds with the filled skutterudite structure were discovered by Jeitschko and Braun in 1977 (4) and have the general formula  $\text{RM}_4\text{X}_{12}$ , where R is La, Ce, Pr, Nd, or Eu; M is Fe, Ru, or Os; and X is P, As, or Sb. These compounds are cubic with 34 atoms in the unit cell and space group  $IM\bar{3}$  (Fig. 1). This structure consists of square planar rings of four pnictogen (group VA) atoms (X) with the rings oriented along the (100), (010), or (001) crystallographic directions. The metal (M) atoms form a simple cubic sublattice, and the R atoms are positioned in the two remaining "holes" in the unit cell. X-ray (5) and neutron (6) structure refinements indicate that for many of the compounds, the R atoms (such as La or Ce) tend to exhibit exceptionally large thermal parameters, corresponding to the "rattling" of these atoms in an oversized atomic cage. As shown below, this rattling markedly reduces the thermal conductivity of these filled skutterudite compounds. A similar effect has been observed in crystalline materials in which the local vibration of an atom or molecule in the structure reduces the thermal conductivity to values expected for an amorphous solid of the same chemical composition (3, 7). When the R atoms are absent from the structure, the basic skutterudite structure is formed.

Since the original papers of Jeitschko and Braun, many other variations of mate-

rials with this structure have been synthesized (8–10). Because these compounds are difficult to synthesize in pure form, the solid-state properties of most of these materials are unknown. Those compounds that have been successfully investigated, however, include several superconductors (11), a heavy-fermion metal (12), Kondo-like narrow-gap semiconductors (8), a ferromagnet (8), and, in the present case, narrow-gap semiconductor with moderate mobilities. Although our original motivation for the synthesis of these materials was to investigate the thermoelectric properties of so-called Kondo insulators (13), reports on the thermoelectric properties of binary skutterudite compounds, such as  $\text{IrSb}_3$ ,  $\text{RhSb}_3$ , and  $\text{CoSb}_3$  (14–18), shifted our focus to more traditional narrow-gap semiconductors with the filled skutterudite structure.

The binary skutterudite antimonides exhibit excellent electrical transport properties, including some of the highest values for hole mobility ever reported for a semiconductor (16). Unfortunately, the thermal conductivities of these binary antimonides are much too large for thermoelectric applications (17). Ternary semiconductors with the filled skutterudite structure provide another degree of freedom in optimizing thermoelectric properties relative to their binary counterparts. The electronic conduction in these materials appears to occur mainly in the Sb orbitals that are spatially separated from the rattling atom (19). In these materials, the possibility exists to create what Slack (3) has termed an "electron crystal" and a "phonon glass." In theory, such a material would exhibit superior ther-

moelectric performance. The work discussed below represents our efforts toward creating such a material.

We prepared the compounds  $\text{CeFe}_{4-x}\text{Co}_x\text{Sb}_{12}$  and  $\text{LaFe}_{4-x}\text{Co}_x\text{Sb}_{12}$  by melting stoichiometric quantities of the highest purity elements in carbon-coated, sealed, evacuated silica tubes at temperatures of 1000° to 1100°C for 24 to 48 hours. The reactive rare-earth elements (99.99% pure electropolished rods) were added to the silica tubes in a helium dry box to avoid the formation of the rare-earth oxide. The silica tubes were removed from the furnace at high temperature and quenched in a water bath. The samples were then annealed at 700°C for several days. The prereacted material was ball-milled to a fine powder and hot-pressed into a dense polycrystalline solid. Depending on the exact

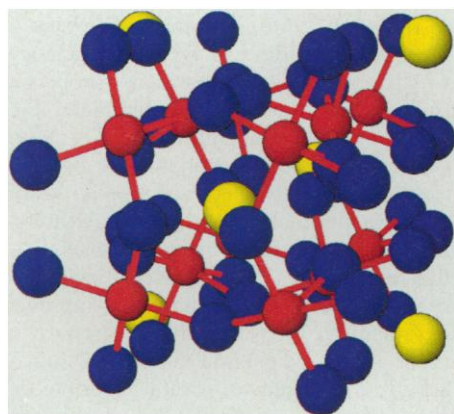


**Fig. 1.** Atomic structural model of the filled skutterudite compounds  $\text{CeFe}_{4-x}\text{Co}_x\text{Sb}_{12}$  and  $\text{LaFe}_{4-x}\text{Co}_x\text{Sb}_{12}$ . The Sb atoms are depicted in blue, Fe or Co atoms in red, and La or Ce in yellow. Only the shortest Sb–transition metal bonds (2.55 Å) are shown for clarity. The relatively large "atomic cage" surrounding the rare-earth ion is evident. The vibration of the rare-earth ion in this cage markedly reduces the thermal conductivity of these materials.

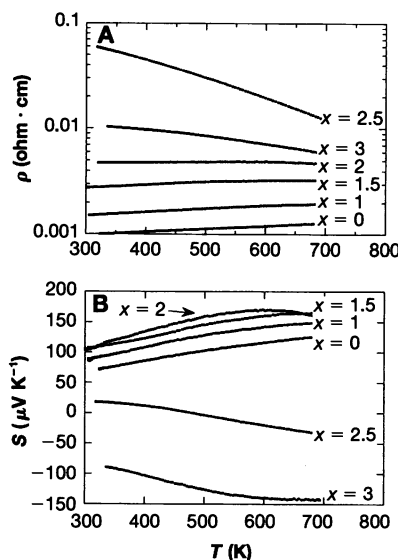


**Fig. 2.** Transport properties of  $\text{CeFe}_{4-x}\text{Co}_x\text{Sb}_{12}$  alloys: (A) resistivity  $\rho$  versus temperature  $T$  for alloys with different Co concentrations; (B) thermopower  $S$  versus  $T$  for the same set of alloys as in (A).

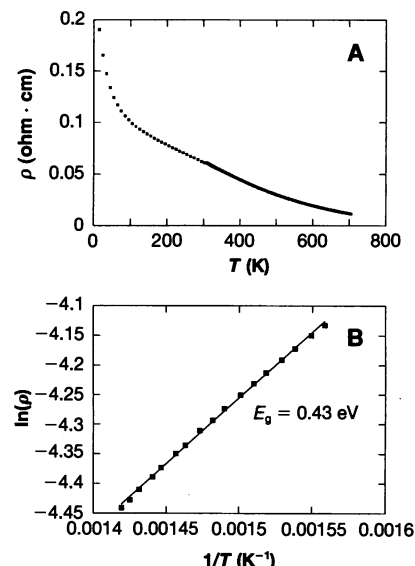


**Fig. 3.** (A) Plot of  $\rho$  versus  $T$  data for a  $\text{CeFe}_{1.5}\text{Co}_{2.5}\text{Sb}_{12}$  alloy; (B) natural logarithm of  $\rho$  versus  $1/T$  for the high-temperature data shown in (A). These data indicate a semiconducting transport gap of 0.43 eV.

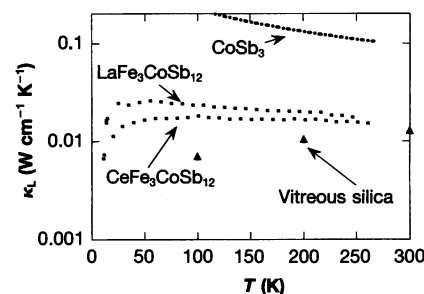


**Fig. 4.** Lattice thermal conductivity data for  $\text{LaFe}_3\text{CoSb}_{12}$ ,  $\text{CeFe}_3\text{CoSb}_{12}$ , and  $\text{CoSb}_3$ . The Wiedemann-Franz law has been used to subtract the electronic contribution to the thermal conductivity. The thermal conductivity values shown correspond to zero porosity. Also shown for comparison is the thermal conductivity of vitreous silica (triangles).

conditions used in the synthesis process, single-phase solids with densities between 75 and 95% of the theoretical x-ray density were obtained. The lattice constants of these compounds were linear with the Co concentration  $x$ , although at high Co concentrations the x-ray patterns indicated incomplete filling of the rare-earth site.

The electrical resistivity and thermopower for a family of  $\text{CeFe}_{4-x}\text{Co}_x\text{Sb}_{12}$  compounds, respectively, are shown in Fig. 2, A and B. The composition given corresponds to the starting composition. The motivation for replacing Fe by Co is due in part to our earlier experimental work on the doping of  $\text{CoSb}_3$  semiconductors (17). Because Co has one more outer electron than Fe, it should fill the holes in the relevant valence band, resulting in a semiconductor with a gap similar to that of  $\text{CoSb}_3$  (0.5 eV). This simple picture is complicated, however, by the tendency of this structure to reject part of the Ce from the R sites with increasing Co content. Nevertheless, the data shown in Fig. 2 tend to qualitatively validate this simple picture. As Co is substituted for Fe, both the resistivity and the thermopower increase, corresponding to the filling of valence band holes and the lowering of the carrier concentration. At a Co concentration of  $x = 2.5$ , semiconducting behavior is clearly observed in the resistivity (Fig. 3A). Analysis of the high-temperature portion of the resistivity data [ $\rho = A \exp(E_g/2T)$ , where  $A$  is a constant and  $E_g$  is the semiconducting gap], shown in Fig. 3A indicate  $E_g = 0.43$  eV, a value close to that found by us and others for  $\text{CoSb}_3$  (Fig. 3B) (14, 17). For alloys with values of  $x$  greater than 2.5, the thermopower becomes negative as electrons begin to fill the conduction band. Hall data taken on these samples are consistent with this model. The description should not be taken too literally, however, because these compounds have 34 atoms per unit cell, and band structure calculations from similar ma-

terials indicate numerous relevant bands near (and in one case through) the semiconducting gap (19). Many more experiments and calculations are required before a clear understanding of these interesting materials will emerge. For this initial set of samples, a Co concentration corresponding to  $x = 1$  had the largest value of  $ZT$  ( $\sim 0.7$  at 800 K). If the rare-earth valence is the normal value of +3, this composition ( $\text{CeFe}_3\text{CoSb}_{12}$  or  $\text{LaFe}_3\text{CoSb}_{12}$ ) should formally be isoelectronic with semiconducting  $\text{CoSb}_3$ .

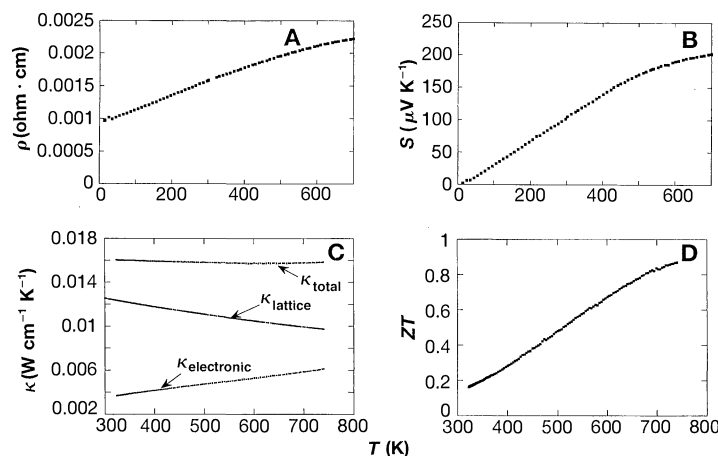
The low-temperature thermal conductivity data for  $\text{LaFe}_3\text{CoSb}_{12}$  and  $\text{CeFe}_3\text{CoSb}_{12}$  are compared to data from  $\text{CoSb}_3$  and vitreous silica in Fig. 4. Relative to  $\text{CoSb}_3$ , the filled skutterudites exhibit a remarkable decrease of one order of magnitude in  $\kappa_L$ , the lattice thermal conductivity, and reach a value at room temperature equivalent to that of vitreous silica (7). At room temperature, the ratio of  $\kappa_L$  to  $\kappa_e$ , the electronic thermal conductivity, is  $\sim 2.5$  for the filled skutterudite as compared with 17 for  $\text{CoSb}_3$ . These thermal conductivity values are comparable to those recently obtained by others on similar filled skutterudite materials (9, 12). Such low values for  $\kappa_L$  are primarily a result of the effectiveness of the rattling rare-earth ions in scattering phonons (3, 9, 12). At temperatures near 50 K, the thermal conductivity of the Ce compound is significantly lower than that of the La compound. Most of this difference is caused by the proximity of the Ce level to the Fermi energy (20). This additional magnetic scattering mechanism may be useful if these materials can be tailored for refrigeration applications near liquid  $\text{N}_2$  temperatures (77 K).

Above room temperature, the thermal conductivity of  $\text{CeFe}_3\text{CoSb}_{12}$  is slightly lower than that of  $\text{LaFe}_3\text{CoSb}_{12}$ , but the larger thermopower of  $\text{LaFe}_3\text{CoSb}_{12}$  more than compensates for this difference and results in a value of  $ZT$  near 1 ( $0.9 \pm 0.2$ ) at 800 K (Fig. 5D). This value is comparable to the

highest value obtained for any thermoelectric material. The resistivity, thermopower, and thermal conductivity for  $\text{LaFe}_3\text{CoSb}_{12}$  are also shown in Fig. 5, A through C. The thermal conductivity data from 300 to 400 K are accurate to  $\pm 2\%$  (21); the thermal conductivity data from 400 to 800 K were determined from thermal diffusivity measurements made with a commercial (22) laser-flash instrument and are accurate to  $\sim 10\%$ . Both the resistivity and the thermopower data are accurate to  $\sim 10\%$ . The peritectic decomposition of  $\text{LaFe}_3\text{CoSb}_{12}$  at  $\sim 1050$  K precludes the use of this material at extremely high temperatures.

Hall data at room temperature and at liquid  $\text{N}_2$  temperature were obtained on several  $\text{CeFe}_3\text{CoSb}_{12}$  and  $\text{LaFe}_3\text{CoSb}_{12}$  samples. The apparent carrier concentrations were in the range from  $1 \times 10^{20}$  to  $5 \times 10^{21} \text{ cm}^{-3}$  with mobilities between 2 and  $30 \text{ cm}^2 \text{ V}^{-1} \text{ s}^{-1}$ . In all cases, the mobilities increased with decreasing temperature, which suggested that thermal vibrations of the lattice provide the dominant scattering mechanism for carriers. The mobilities also increased significantly as the carrier concentration was reduced, which implies that larger values of  $ZT$  can be attained at lower temperatures. Controlling the carrier concentrations in these materials by means of our synthesis method is difficult. For example, a 1% change in the rare-earth concentration translates into a change in carrier concentration of  $0.7 \times 10^{20} \text{ cm}^{-3}$ . However, assuming scattering by acoustic phonons, parabolic bands, and modeling of the transport properties by means of the Boltzmann approximation [see (1), pp. 58–63], we estimate that a maximum  $ZT$  value of 1.4 can be obtained at 1000 K with a properly optimized (that is, correct carrier concentration)  $\text{LaFe}_3\text{CoSb}_{12}$  sample. Preparation of single crystals of these materials by a flux growth technique or through laser ablation appears to be a more promising approach, both for understanding the physics and for producing samples with higher  $ZT$ .

**Fig. 5.** Electrical and thermal transport data from a  $\text{LaFe}_3\text{CoSb}_{12}$  sample. (A) Plot of  $\rho$  versus  $T$ ; (B) plot of  $S$  versus  $T$ ; (C) plot of  $\kappa$  versus  $T$ ; (D) plot of  $ZT$  versus  $T$ . The total thermal conductivity along with the approximate lattice and electronic contributions are shown versus temperature in (C). The resistivity and thermal conductivity data have not been corrected for sample porosity because  $ZT$  does not depend on porosity.



## REFERENCES AND NOTES

- H. J. Goldsmid, *Electronic Refrigeration* (Pion, London, 1986).
- C. Wood, *Rep. Prog. Phys.* **51**, 459 (1988).
- G. A. Slack, *Thermoelectric Handbook* (Chemical Rubber, Boca Raton, FL, in press).
- W. Jeitschko and D. Braun, *Acta Crystallogr.* **B33**, 3401 (1977).
- D. J. Braun and W. Jeitschko, *J. Less Common Met.* **72**, 147 (1980).
- B. C. Chakoumakos, B. C. Sales, D. G. Mandrus, unpublished data.
- D. G. Cahill, S. K. Watson, R. O. Pohl, *Phys. Rev. B* **46**, 6131 (1992).
- G. P. Meisner, M. S. Torikachvili, K. N. Yang, M. B. Maple, R. P. Guertin, *J. Appl. Phys.* **57**, 3073 (1985).
- G. S. Nolas, G. A. Slack, D. T. Morelli, T. M. Tritt, A. C. Ehrlich, *J. Appl. Phys.*, in press.
- N. T. Stetson, S. M. Kauzlarich, H. Hope, *J. Solid State Chem.* **91**, 140 (1991).
- G. P. Meisner, *Physica B* **108**, 763 (1981); L. E.

- DeLong and G. P. Meisner, *Solid State Commun.* **53**, 119 (1985).
12. D. T. Morelli and G. P. Meisner, *J. Appl. Phys.* **77**, 3777 (1995).
13. Z. Fisk, P. C. Canfield, J. D. Thompson, M. F. Hundley, *J. Alloys Compounds* **181**, 369 (1993); B. C. Sales *et al.*, *Phys. Rev. B* **50**, 8207 (1994).
14. T. Caillat, A. Borshchevsky, J.-P. Fleurial, in *Proceedings of the 11th International Conference on Thermoelectrics*, K. R. Rao, Ed. (Univ. of Texas at Arlington Press, Arlington, 1993), pp. 98–102.
15. G. A. Slack and V. G. Tsoukala, *J. Appl. Phys.* **76**, 1665 (1994); D. Mandrus *et al.*, *Phys. Rev. B* **52**, 4926 (1995); J.-P. Fleurial, T. Caillat, A. Borshchevsky, in *Thirteenth International Conference on Thermoelectrics*, B. Mathiprakasam and P. Heenan, Eds. (AIP Conference Proceedings No. 316, American Institute of Physics, New York, 1995), pp. 40–44.
16. D. T. Morelli *et al.*, *Phys. Rev. B* **51**, 9622 (1995).
17. J. W. Sharp, E. C. Jones, R. K. Williams, P. M. Martin, B. C. Sales, *J. Appl. Phys.* **78**, 1013 (1995).
18. F. Hulliger, *Helv. Phys. Acta* **34**, 782 (1961); D. Dudkin and N. K. Abrikosov, *Sov. Phys. Solid State* **1**, 126 (1959).
19. D. Jung, M.-H. Whangbo, S. Alvarez, *Inorg. Chem.* **29**, 2252 (1990); D. J. Singh and W. E. Pickett, *Phys. Rev. B* **50**, 11235 (1994).
20. B. C. Sales, unpublished data.
21. R. K. Williams, R. K. Nanstad, R. S. Graves, R. G. Berggren, *J. Nucl. Mater.* **115**, 211 (1983).
22. Flashline-5000 (Anter Corporation, Pittsburgh, PA). The data from this instrument were calibrated with a

National Institute of Standards and Technology stainless steel standard.

23. Sponsored in part by a Cooperative Research and Development Agreement with Marlow Industries, contract CRADAX94-0324, and in part by the Division of Materials Sciences, U.S. Department of Energy contract DE-ACO5-96OR22464. We thank H. B. Lyon, J. W. Sharp, G. A. Slack, J.-P. Fleurial, T. Caillat, J. O. Sofo, and G. D. Mahan for illuminating discussions; R. B. Dinwiddie and H. Wang for thermal diffusivity measurements on several samples from 300 to 800 K; and P. M. Martin for helping with the precise thermal conductivity measurements near room temperature.

23 January 1996; accepted 19 March 1996

## Crystal Structure of the Dual Specificity Protein Phosphatase VHR

Jirundon Yuvaniyama, John M. Denu, Jack E. Dixon, Mark A. Saper\*

Dual specificity protein phosphatases (DSPs) regulate mitogenic signal transduction and control the cell cycle. Here, the crystal structure of a human DSP, vaccinia H1-related phosphatase (or VHR), was determined at 2.1 angstrom resolution. A shallow active site pocket in VHR allows for the hydrolysis of phosphorylated serine, threonine, or tyrosine protein residues, whereas the deeper active site of protein tyrosine phosphatases (PTPs) restricts substrate specificity to only phosphotyrosine. Positively charged crevices near the active site may explain the enzyme's preference for substrates with two phosphorylated residues. The VHR structure defines a conserved structural scaffold for both DSPs and PTPs. A "recognition region," connecting helix  $\alpha 1$  to strand  $\beta 1$ , may determine differences in substrate specificity between VHR, the PTPs, and other DSPs.

The protein encoded by the H1 open reading frame in vaccinia virus was identified as the first dual specificity protein phosphatase (DSP), capable of hydrolyzing phosphate monoesters from peptides containing either phosphotyrosine or phosphoserine (1). The p80<sup>CDC25</sup> protein, which is necessary for regulating the M phase transition during the cell cycle (2), showed limited sequence identity to the vaccinia phosphatase (3). The p80<sup>CDC25</sup> protein has intrinsic phosphatase activity and activates the p34<sup>CDC2</sup>-cyclin protein kinase complex by dephosphorylating adjacent residues Thr<sup>14</sup> and Tyr<sup>15</sup> (4).

More than 20 mammalian DSPs have now been identified. Two of them, MKP-1 (5) and PAC-1 (6), regulate mitogenic signal transduction by dephosphorylating both Thr<sup>183</sup> and Tyr<sup>185</sup> residues on the mitogen-activated protein (MAP) kinase (5, 7). A vaccinia H1-related phosphatase (VHR) was identified in humans and shown to be a DSP (8). VHR can hydrolyze phosphoty-

rosine and phosphothreonine residues on peptides derived from MAP kinase (9) and can activate maturation promotion factor when injected into *Xenopus* oocytes (10). Mutagenesis of Cys<sup>124</sup> abolished all phosphatase activity, which suggests that the enzyme contains a single active site (8). Recombinant VHR is the archetypal phosphatase used in studies designed to elucidate the catalytic mechanism of the DSPs (11–14).

To understand the structural determinants of specificity and function of this enzyme family, we solved the three-dimensional structure of VHR to 2.1 Å resolution by x-ray crystallography (15) (Table 1). A typical example of the "omit" electron density map is presented in Fig. 1. VHR consists of a single  $\alpha + \beta$ -type domain of dimensions 50 Å by 40 Å by 32 Å. The loop between the  $\beta 8$  strand and  $\alpha 5$  helix (residues 123 to 131) (Fig. 1, also Fig. 4A) contains the consensus active-site sequence His-Cys-X-X-Gly-X-X-Arg-(Ser or Thr) (16) with the catalytic Cys<sup>124</sup> thiol at its center (X is any amino acid). In the crystal structure, the competitive inhibitor sulfate is bound at the active site (Fig. 1). The oxygen atoms of sulfate form hydrogen bonds to the main chain amides of the active site loop and to the Arg<sup>130</sup> side chain, mimicking the corresponding inter-

actions between the phosphate oxygens on a phosphoprotein substrate.

To explore the structural basis for how VHR can bind and dephosphorylate either phosphotyrosine, phosphothreonine, or phosphoserine residues, we compared the active sites of VHR and those of two protein tyrosine phosphatases (PTPs), *Yersinia* PTP (17, 18) and human PTP1B (19, 20). The specificity of PTP1B for phosphotyrosine, and not for phosphothreonine, is determined primarily by the depth of the active site cleft (20). Although the active site loop, termed the P-loop in the *Yersinia* enzyme, is structurally conserved among both PTPs and DSPs, cross sections of the VHR and the *Yersinia* PTP active sites revealed a disparity in the depth of the active site clefts (Fig. 2). The active site pocket of VHR is at most 6 Å deep and is surrounded by side chains mainly from the P-loop itself. In contrast, the depth of the *Yersinia* PTP and PTP1B (20) active site cleft is about 9

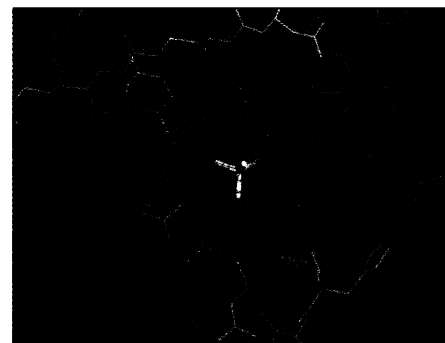


**Fig. 1.** VHR catalytic site with the P-loop (magenta) containing the catalytic Cys<sup>124</sup> and a bound sulfate anion (yellow) (33). Hydrogen bonds are shown in dashed lines. The main chain amides of the P-loop make six additional hydrogen bonds (not shown) with the three sulfate oxygens. Contoured at 2.3 $\sigma$  (dark green) is a 2.1 Å resolution "omit" map in which the P-loop atoms and sulfate were not included in the simulated-annealing refinement before map calculation. Portions of the structure are similarly colored in all figures: the general acid loop (residues 88 to 98) between  $\beta 7$  and  $\alpha 4$  is blue, the  $\alpha 1$ - $\beta 1$  or "recognition region" (residues 19 to 29) is green, and the "variable insert" between  $\beta 3$  and  $\beta 7$  (residues 62 to 82) is orange. Red shows Arg<sup>158</sup>.

J. Yuvaniyama and M. A. Saper, Biophysics Research Division and Department of Biological Chemistry, University of Michigan, Ann Arbor, MI 48109–1055, USA. J. M. Denu and J. E. Dixon, Department of Biological Chemistry, University of Michigan, Ann Arbor, MI 48109–0606, USA.

\*To whom correspondence should be addressed. E-mail: saper@umich.edu